Human Molecular Genetics, 2000, Vol. 9, No. 5 849–858

# Nuclear targeting defect of SMN lacking the C-terminus in a mouse model of spinal muscular atrophy

**Tony Frugier[+,§], Francesco D. Tiziano[+,§], Carmen Cifuentes-Diaz[+,§], Pierre Miniou, Natacha Roblot[§], Andrée Dierich, Marianne Le Meur and Judith Melki[§,¶]**

Institut de Génétique et de Biologie Moléculaire et Cellulaire, INSERM, CNRS, ULP, BP163, 67404 Illkirch cedex, CU de Strasbourg, France

Received 4 January 2000; Revised and Accepted 25 January 2000

**Deletion of the murine survival of motor neuron gene (*SMN*) exon 7, the most frequent mutation found in spinal muscular atrophy (SMA) patients, directed to neurons but not to skeletal muscle, enabled generation of a mouse model of SMA providing evidence that motor neurons are the primary target of the gene defect. Moreover, the mutated SMN protein (SMNΔC15) is dramatically reduced in the motor neuron nuclei and causes a lack of gems associated with large aggregates of coilin, a coiled-body-specific protein. These results identify the lack of the nuclear targeting of SMN as the biochemical defect in SMA.**

## INTRODUCTION

Spinal muscular atrophy (SMA) is a neuromuscular disorder characterized by degeneration of motor neurons of the spinal cord associated with symmetrical limb and trunk paralysis with muscle atrophy. SMA represents a frequent recessive autosomal disorder and is one of the most common genetic causes of death in childhood (1,2). A positional cloning strategy allowed the identification of the survival of motor neuron gene (*SMN*) as the SMA-determining gene (3,4). *SMN* exists in duplicate, with only five nucleotides distinguishing it from its highly homologous copy gene, *SMN^c^* (4–6). In SMA, 95% of patients carry homozygous deletion or conversion events of the *SMN* exon 7 and the remaining 5% carry intragenic mutations within the *SMN* gene (reviewed in ref. 7). *SMN* encodes a protein of 294 amino acids which locates both to the cytoplasm and to a nuclear structure called a gem (for gemini of coiled bodies) (8). SMN forms part of a large protein complex that contains the SMN-interacting protein 1 (SIP1) and Sm proteins of the spliceosomal uridine-rich small ribonucleoproteins suggesting that SMN plays a key role in spliceosomal biogenesis by bringing together the components of the spliceosomal complex (8–11).

In contrast to the human, the mouse *SMN* gene is not duplicated, which may explain the fact that the conventional knockout of the *SMN* gene results in embryonic lethality (12–14). To gain insight into the pathogenesis of SMA and to understand the function of SMN inferred from the SMA phenotype, we carried out a conditional deletion of the murine *SMN* exon 7, the most frequent mutation found in SMA patients, using the Cre/loxP recombination system of bacteriophage P1 (15,16).

## RESULTS

### Homozygous deletion of *SMN* exon 7 in all cell types results in early embryonic lethality

We used a targeting vector that includes two loxP sites flanking the *SMN* exon 7 and a *NeoR* gene (Fig. 1). Through homologous recombination, mice heterozygous or homozygous for the loxP-flanked *SMN* exon 7 allele (*SMN^F7^*) appear similar in size and morphology to wild-type mice. At the RNA level, no alternative splicing of *SMN* exon 7 was detected by RT–PCR amplification analysis of RNA extracted from various tissues of the *SMN^F7/F7^* mice, indicating that neither the *NeoR* gene nor the loxP sites have a deleterious effect on *SMN* splicing (Fig. 2). Mice heterozygous for the *SMN^F7^* allele were initially crossed with a strain carrying the *Cre* recombinase transgene driven by the cytomegalovirus (CMV) promoter (17). Cre recombinase expression in germline led to the generation of mice carrying a heterozygous deletion of *SMN* exon 7 (*SMN^Δ7/+^*). *SMN^Δ7/+^* mice gained weight normally after birth and have remained indistinguishable from wild-type littermates to date (12 months of age). Histological examination of skeletal muscle did not reveal any morphological changes (data not shown). The Cre-mediated deletion of the *SMN* exon 7 resulted in *SMN* transcripts lacking exon 7 as determined by sequencing of RT–PCR amplification products of RNA extracted from various tissues including the spinal cord and skeletal muscle of *SMN^Δ7/+^* mice (Fig. 2). To determine whether the homozygous deletion of *SMN* exon 7 in all cell types would lead to embryonic lethality or to a milder phenotype, *SMN^Δ7/+^* mice were intercrossed. These crosses generated no live *SMN^Δ7/Δ7^* mice out of 50 newborns analysed (Table 1). To determine the timing of the *SMN^Δ7/Δ7^* lethality, embryos were analysed during gestation. At 9 days post-coitum, a total of 53 embryos, including 13 with almost complete resorbtion was analysed (Fig. 2). Normal embryos showed the expected ratio

[+]These authors contributed equally to this work
[§]Present address: Laboratoire de Neurogénétique Moléculaire, INSERM E9913, GENOPOLE, 2 rue Gaston Crémieux CP 5724, 91057 Evry cedex, France
[¶]To whom correspondence should be addressed. Tel: +33 1 60 87 45 52; Fax: +33 1 60 87 45 50; Email: j.melki@genopole.inserm.fr

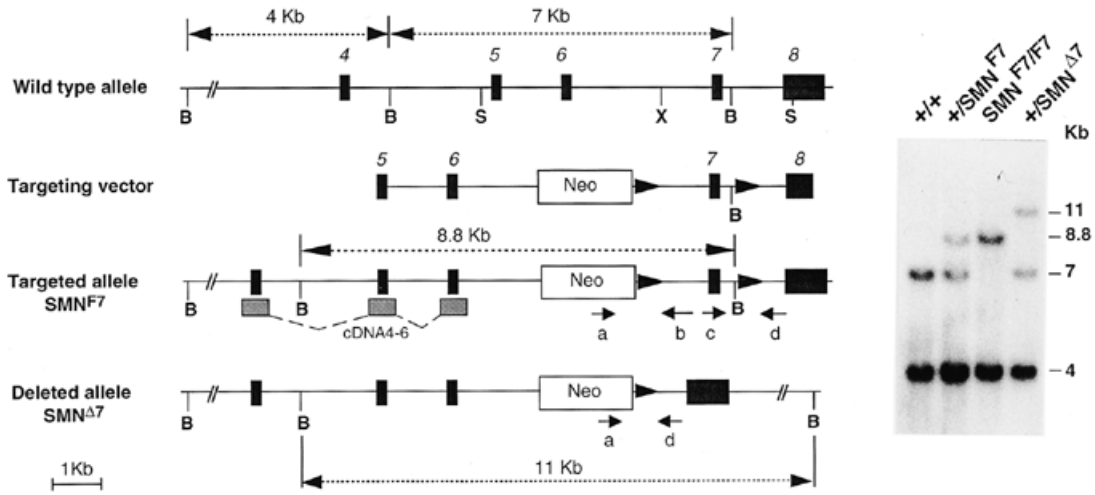


**Figure 1.** Conditional mutagenesis of mouse *SMN* exon 7. (Left) The wild-type genomic *SMN* locus surrounding the targeted exon, the targeting vector, the loxP-flanked *SMN* exon 7 allele ($SMN^{F7}$) and the Cre-mediated deleted allele ($SMN^{\Delta7}$). Filled rectangles indicate exons and filled arrows indicate the position of loxP sequences. The locations of the PCR primers used to screen for homologous recombination or Cre-mediated deletion and the cDNA probe used to confirm this are also given. B, *Bam*HI; X, *Xho*I; S, *Sal*I; Neo, neomycine resistance cassette gene. Primers: a, *PHR5*; b, *XG3*; c, *ex7sou1*; d, *GS8*. (Right) Southern blot analysis of DNA from tail biopsies of wild-type (+/+), $SMN^{F7/+}$, $SMN^{F7/F7}$ and $SMN^{\Delta7/+}$ mice. Digestion with *Bam*HI generates a 7 kb wild-type fragment, an 8.8 kb 'floxed' fragment and a 11 kb deleted fragment which are detected with a probe derived from *SMN* cDNA and containing exons 4–6. An additional fragment of 4 kb corresponding to a more upstream restriction fragment is detected in wild-type, 'floxed' and deleted alleles using the same probe.

for genotypes (+/+) or ($SMN^{\Delta7/+}$), whereas all resorbed embryos were homozygous for the $SMN^{\Delta7}$ mutation (Fig. 2 and Table 1) indicating that homozygous deletion of *SMN* exon 7 in all cell types results in embryonic lethality during early development.

## Homozygous deletion of *SMN* exon 7 directed to neurons leads to the generation of mice affected with an SMA phenotype

To induce neuron-restricted exon 7 deletion, we generated transgenic mice harbouring the *Cre* recombinase gene driven by the promoter of the rat neuron-specific enolase gene (*NSE*) (18). The transgenic NSE-Cre lines (NSE-23 and -39) were crossed to the strain harbouring the $SMN^{F7}$ allele and Cre-mediated deletion of *SMN* exon 7 was quantified through semi-quantitative PCR amplification analyses of genomic DNA extracted from various tissues of double transgenic mice (*NSE-Cre*, $SMN^{F7/+}$). Of the two lines, only one, NSE39-Cre, generated a high level of Cre-mediated exon excision in neuronal tissues and this line was studied further (Fig. 3). *In situ* hybridization using a *Cre* recombinase riboprobe was performed and revealed an expression pattern that was restricted to neurons in the adult spinal cord whereas in skeletal muscle, no Cre recombinase expression was detected (Fig. 3). These findings led us to use the NSE39-Cre transgenic line for the conditional targeting of *SMN* in neurons but not in the skeletal muscle.

NSE39-Cre mice were crossed with mice carrying an $SMN^{\Delta7}$ allele. $F_1$ offspring carrying both the *NSE39-Cre* transgene and $SMN^{\Delta7}$ allele were selected and crossed with $SMN^{F7/F7}$ mice. Twenty-eight of 105 (26.6%) mice carried both the *NSE39-Cre* recombinase transgene and the $SMN^{F7/\Delta7}$ genotype as expected (termed $SMN^{F7/\Delta7}$, $Cre^{+}$). Mice carrying this genotype can be easily distinguished from their control littermates by severe motor defect associated with tremors, both of which are evident at 2 weeks of age (Fig. 4). Mutant mice exhibit an extremely reduced life expectancy, dying at a mean age of 25 days (range 17–36 days, $n = 10$). Morphological analysis on transverse sections of several skeletal muscles including gastrocnemius, intercostal and sternomastoid revealed the presence of groups of atrophic muscle fibers and angular fibers intermixed with normal-sized fibers in $SMN^{F7/\Delta7}$, $Cre^{+}$ mice using haematoxylin and eosin staining (Fig. 5). These findings are consistent with a denervation of skeletal muscles of neurogenic origin which was further confirmed by the presence of a marked extrajunctional labeling of acetylcholine receptors in $SMN^{F7/\Delta7}$, $Cre^{+}$ animals (Fig. 5). A morphological analysis on transverse semithin sections of spinal cord was performed on 2-week-old control and $SMN^{F7/\Delta7}$, $Cre^{+}$ mice using toluidine blue staining. In mutant mice, the striking feature was the pronounced morphological changes of nuclei of motor neurons (Fig. 5). A marked increase in toluidine blue staining was observed within the nuclei at the nucleo-cytoplasmic boundary suggesting the presence of indentations of the nuclear membrane (Fig. 5). In addition, some motor neurons display a granular aspect of the cytoplasm (Fig. 5). To determine whether these changes were associated with a loss of motor neurons, a quantification of motor neuron number was performed at the lumbar level of the spinal cord but no significant loss of motor neurons of the anterior horns was detected in 2-week-old mutant mice (data not shown). In 4-week-old $SMN^{F7/\Delta7}$, *Cre+* mice, toluidine blue or DAPI staining of spinal cord sections revealed the presence of vacuolation of the cytoplasm associated with a marked deformation or fragmentation of motor neuron nuclei (Fig. 6).

## Prominent and frequent indentations of the nuclear membrane are associated with the lack of gems associated with large aggregates of coilin in motor neuron nuclei

To test whether the neuromuscular changes are associated with an abnormal expression of *SMN* transcript, RT–PCR amplification analysis of RNA extracted from the spinal cord

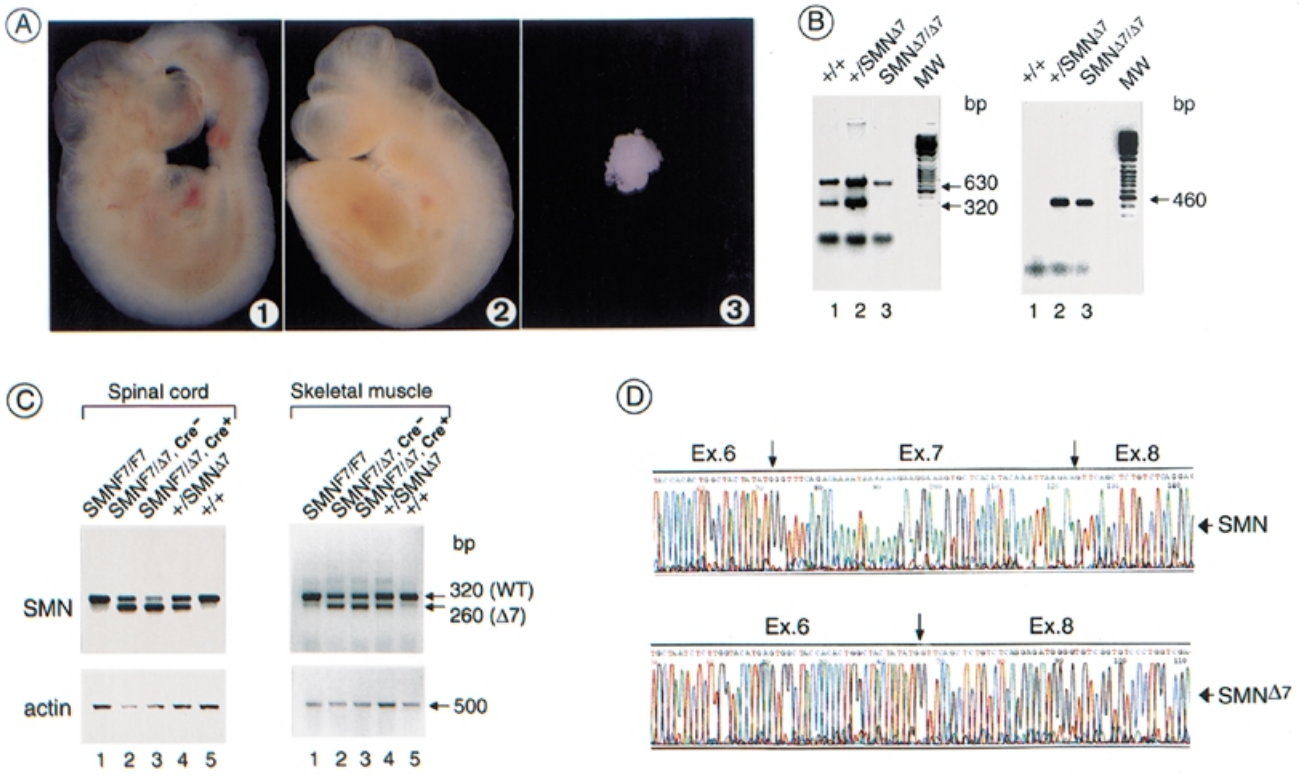


**Figure 2.** Deletion of *SMN* exon 7 in all cell types. (**A**) Nine day post-coitum embryos belonging to the same litter of $SMN^{\Delta7/+}$ intercrosses are shown at the same magnification. (1) +/+; (2) $SMN^{\Delta7/+}$; (3) $SMN^{\Delta7/\Delta7}$. (**B**) Genotype analysis of DNA extracted from the corresponding yolk sacs using PCR amplification. (Left) Primers *int7b* (5′-CTC ACA GAG ATC CTC TTG CCC TGA-3′) and *ex7sou2* (5′-AAT TTG TAT GTG AGC ACT TTC CTT CT-3′) located upstream of and within exon 7, respectively, were used to amplify the wild-type fragment (320 bp). PCR amplification using primers flanking *SMN* exon 4 was used as internal positive control (630 bp). (Right) Detection of the $SMN^{\Delta7}$ allele by PCR amplification using primers *pHR5* and *GS8* generating a 460 bp fragment derived from the deleted allele only. (**C**) Transcript analysis of *SMN* from spinal cord or skeletal muscle tissues. RT–PCR amplification of *SMN* was performed on total RNA using primers flanking *SMN* exon 7 and located in exons 6 (*ex6.5*, 5′-ATA ATC CCG CCA CCC CCT-3′) and 8 (*ex8sou*, 5′-GGC ACG CTC TGC TGC TGA CTT AG-3′). RT–PCR amplification reveals the *SMN* transcripts retaining (320 bp) or lacking (260 bp) exon 7. Note the slight increase of the truncated transcript in both spinal cord and skeletal muscle of $SMN^{F7/\Delta7}$, $Cre^{-}$ mice when compared with the RNA pattern of $SMN^{\Delta7/+}$ mice. A marked reduction in the amount of full-length *SMN* transcript is detected in spinal cord but not in skeletal muscle of $SMN^{F7/\Delta7}$, $Cre^{+}$ mice compared with that observed in mice harbouring the other genotypes. RT–PCR of α-actin transcripts was used as an internal control. (**D**) Sequence analysis of the RT–PCR products generated from RNA of $SMN^{\Delta7/+}$ mice. Full-length and truncated *SMN* transcripts were separated on an 8% polyacrylamide gel, excised and reamplified using the same primers prior to direct sequencing. Arrows indicate the boundaries of each exon.

**Table 1.** *SMN* gene analysis in adult and 9 day post-coitum embryos of $+/SMN^{\Delta7}$ mouse intercrosses

| Genotype | +/+ | $+/SMN^{\Delta7}$ | $SMN^{\Delta7/\Delta7}$ | $\chi^2$ |
|---|---|---|---|---|
| Adults ($n = 50$) | 17 (34%) | 33 (66%) | 0 | 16.68 ($P < 0.001$) |
| 9 day post-coitum embryos ($n = 53$) | 15 (28.3%) | 25 (47.2%) | 13 (24.5%) | 0.32 ($P > 0.8$) |

and skeletal muscle of mutant or wild-type mice was performed using primers flanking *SMN* exon 7 (Fig. 2). The transcript analysis of *SMN* revealed a marked reduction of the full-length transcript associated with an increased amount of the $SMN^{\Delta7}$ transcript in the spinal cord but not in skeletal muscle of $SMN^{F7/\Delta7}$, $Cre^{+}$ mice (Fig. 2). Immunoblotting of proteins prepared from the spinal cord of $SMN^{F7/\Delta7}$, $Cre^{+}$ and control mice was performed using the monoclonal antibody directed against the N-terminal part of the SMN protein (2B1) (8). In $SMN^{F7/\Delta7}$, $Cre^{+}$ mice, the SMN protein is present with an apparent size and amount similar to that observed in control mice (Fig. 7). These results strongly suggest that the truncated *SMN* transcript is translated into a protein lacking the last C-terminal 15 amino acids (SMNΔC15) although the resolution of western blot gel is not sufficient to distinguish the wild-type protein from a protein lacking 15 amino acids. To determine whether the subcellular localization of the truncated protein is similar to that of the wild-type, the monoclonal antibody 2B1 was further used in an immunofluorescence microscopy analysis of spinal cord sections derived from mutant and control mice. In the spinal cord of $SMN^{F7/\Delta7}$, $Cre^{+}$ mice, the 2B1 monoclonal antibody stained the cytoplasm but failed to recognize the localization of SMN in gems of motor neurons (Fig. 7). SIP1, a protein interacting with the N-terminal part of SMN and colocalized with SMN in gems, was immunostained using a monoclonal antibody specific to SIP1 (2E17) (9). In the spinal cord of control mice, SIP1 antibody revealed uniform staining of the nucleus in addition to gems in motor neurons (Fig. 7). In the spinal cord of $SMN^{F7/\Delta7}$, $Cre^{+}$ mice, SIP1 antibody failed to detect gems in motor neurons (Fig. 7). These findings provide strong evidence of an absence of gems in the motor neurons of mutant mice. We therefore tested whether the lack of gems has any effect on the structure or organization of

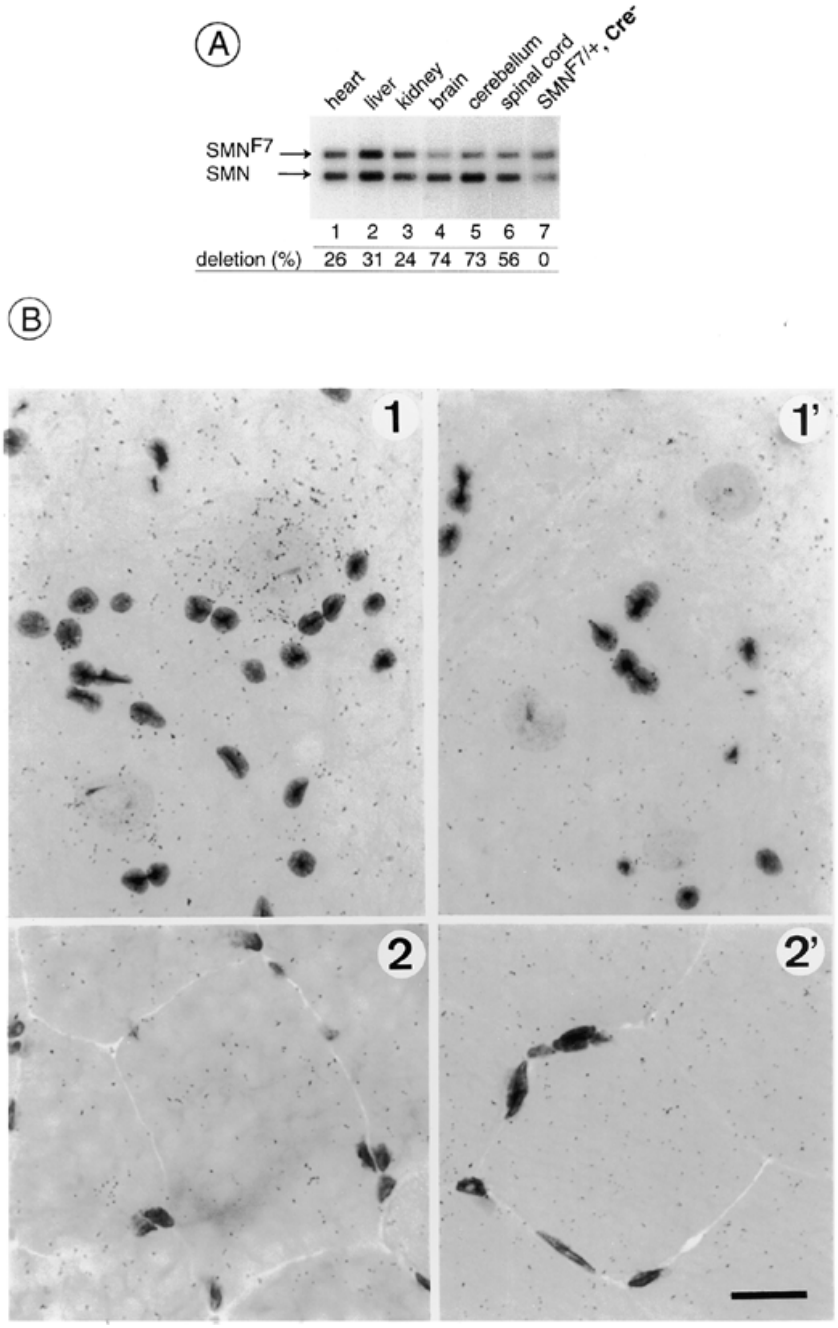


**Figure 3.** Characterization of Cre recombinase activity of the *NSE39-Cre* transgenic line. (**A**) To test the efficiency of DNA excision by the Cre recombinase, *NSE39-Cre* transgenic mice were crossed with mice carrying the $SMN^{F7}$ allele and double transgenic mice were selected (*NSE39-Cre*, $SMN^{F7/+}$). The wild-type and $SMN^{F7}$ alleles were simultaneously amplified by PCR using *ex7sou1* and *GS8*. The efficiency of Cre-mediated deletion was deduced from the ratio of $SMN^{F7}$ to wild-type band intensity in various adult tissues of the double transgenic mouse (lanes 1–6) compared with the ratio in $SMN^{F7/+}$ mouse lacking Cre transgene (lane 7). Cre-mediated deletion is indicated as a percentage. (**B**) *In situ* hybridization using a Cre recombinase riboprobe was performed on spinal cord and skeletal muscle transverse sections counterstained with toluidine blue. Antisense riboprobe reveals an expression pattern restricted to neurons in the adult spinal cord (1) whereas no hybridization signal is detectable in skeletal muscle (2). (1′) and (2′) show the hybridization using the sense riboprobe. Scale bar, 19 μm.

coiled bodies, a nuclear structure most often found to be associated with gems. A polyclonal anti-p80 coilin, a coiled-body-specific protein (19) was used in an immunofluorescence microscopy analysis and detected several small foci corresponding to coiled bodies in motor neuron nuclei of control mouse (Fig. 7). In the spinal cord of $SMN^{F7/\Delta 7}$, $Cre^{+}$ mice, anti-p80 coilin antibody stained large nuclear aggregates providing evidence for a defect in the coilin assembly into coiled bodies (Fig. 7).

## DISCUSSION

Through a conditional gene-targeting approach, we were able to circumvent embryonic lethality resulting from homozygous

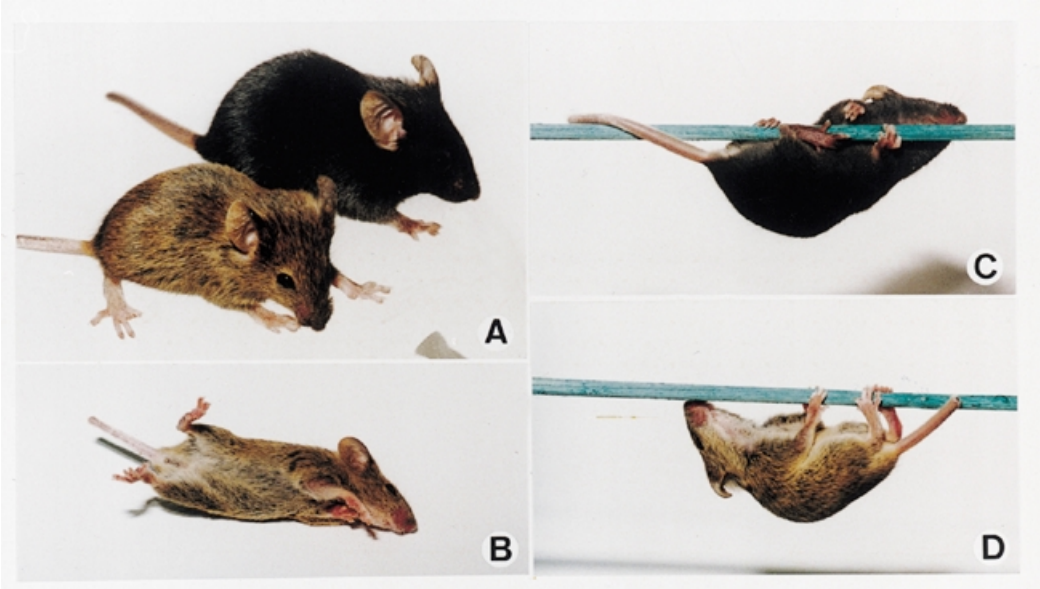


**Figure 4.** Motor defects in ($SMN^{F7/\Delta7}$, $Cre^{+}$) mice. (**A**) Note the abnormal posture of the hindlimbs of the 3-week-old $SMN^{F7/\Delta7}$, $Cre^{+}$ mouse (agouti) compared with the wild-type mouse (black). The mutant mouse has a severe impairment in its ability to right itself when intentionally inverted (**B**) and displays severe hypotonia characterized by a defect of flexor muscles of the limbs and neck when suspended on a horizontal thread (**D**) compared with the posture from the wild-type animal (**C**).

deletion of *SMN* exon 7 in all cell types. The mice carrying a deletion of *SMN* exon 7 directed to neurons display abnormal motor behavior characterized by severe defects in both spontaneous and induced motor activities which are evident at 2 weeks of age. These defects appear to be progressive as mutant mice develop more pronounced motor disability with age and die usually at a mean age of 25 days. Morphological analysis of several skeletal muscles, including those involved in motor activity or respiratory function, revealed the presence of a muscle denervation process of neurogenic origin, a constant feature found in human SMA (20). The morphological analysis of the spinal cords of $SMN^{F7/\Delta7}$, $Cre^{+}$ mice showed the presence of indentations in the motor neuron nuclear membranes which have also been reported to occur with a less pronounced extent in neurodegenerative diseases caused by abnormal polyglutamine repeat expansion (21); however, unlike these diseases no neuronal inclusion was observed in *SMN* mutant mice using toluidine blue staining. In 4-week-old mutant mice, the presence of nuclear fragmentation suggests the presence of an apoptotic process although the abnormal changes of the cytoplasm do not allow exclusion of the involvement of another degenerative process. Further investigations including electron microscopic examination should enable to clarify this point. It is clear that the presence of motor neuron nuclear changes is associated with pronounced neuronal dysfunction as demonstrated by the denervation of skeletal muscle fibers, the targeted cells of motor neurons, despite the absence of motor neuron loss. The morphological changes occurring in response to the lack of SMN have not been reported in human SMA suggesting that they likely represent the early events of neuronal degeneration which lead later to motor neuron loss, a late manifestation such as that found in autopsy material of SMA patients (20). Interestingly, Monani *et al.* (22) found that motor neuron loss is a late manifestation of the disease phenotype of mutant mice that they generated, which is in agreement with our results (22). Previous reports have suggested that a defect of muscular origin might be responsible for motor neuron degeneration in SMA (23,24). Our results demonstrate that an *SMN* gene defect directed to neurons but not to skeletal muscle leads to an SMA phenotype *in vivo* indicating that motor neurons are the primary target of the *SMN* gene defect in SMA. However, it cannot be ruled out that an *SMN* gene defect in both spinal cord and muscle could modulate the SMA phenotype. Conditional *SMN* gene targeting restricted to skeletal muscle or to both spinal cord and skeletal muscle should contribute to further exploring this issue.

The pronounced effect of SMNΔC15 on the organization of both gems and coiled bodies was unexpected. The dramatic reduction of SMNΔC15 within the motor neuron nuclei of mutant mice indicates that the C-terminus of SMN (amino acids 274–288) represents an important domain required for the SMN targeting into gems. Interestingly, the absence of SIP1 assembly into gems strongly suggests that SMN is involved in the normal pathway of gem formation *in vivo*. Previous studies indicated that gems were distinct from coiled bodies, though they were most often found to be closely associated (8). The lack of gems in mutant mice led us to examine coiled body organization. The presence of large nuclear aggregates of coilin indicates that the lack of SMN and/or gems has a pronounced effect on coiled body formation. Therefore, the generation of a mouse model of SMA, carrying the most frequent mutation found in human SMA, allowed us to determine that SMNΔC15 causes a defect in nuclear targeting of SMN which cannot proceed further the normal pathway of gem/coiled body formation, thus identifying the biochemical defect in SMA. In human, coiled bodies were found to be present in SMA fetuses suggesting that the full-length SMN protein which remains present in SMA patients,

but not in mutant mice, is likely able to maintain coiled body structure (25). In human SMA, the highly homologous *SMN^c^* gene remains expressed although the alternative splicing of exon 7 specific to *SMN^c^* transcripts leads to the production of a truncated protein lacking the C-terminus as the murine mutated protein (4,6). Molecular agents able to promote nuclear targeting of the mutant SMN into gems should represent an attractive therapy.

The generation of animal models of SMA required sophisticated genetic strategies to avoid embryonic lethality. In a first strategy, two groups have created mouse lines carrying a transgene which contains the human *SMN^c^* gene (22,26). Mice carrying a low copy number of *SMN^c^* transgene and harbouring a homozygous null *SMN* allele (*SMN^−/−^*) (14,27) develop a severe phenotype consistent with human type I SMA. Crosses of *SMN^−/−^* mice with those carrying a high copy number of *SMN^c^* transgene lead to the absence of abnormal phenotype, which demonstrates that an increased copy number of *SMN^c^* reduces the severity of the phenotype, data consistent with those observed in human SMA. These animal models will be very useful in testing molecules able to upregulate the *SMN^c^* gene (22,26).

The second strategy described in the present study provided important and complementary information: (i) motor neurons are the target cells of the *SMN* gene defect in SMA; (ii) the most frequent gene mutation found in human SMA causes a defect in nuclear targeting of SMN into gems; (iii) the observation of a severe denervation process without marked loss of motor neurons strongly suggests that motor neuron loss is a late manifestation of the disease; and (iv) the mutant mice display an intermediate phenotype resembling human type II or III SMA. They should represent therefore an appropriate model for the design of therapeutic strategies to protect from or prevent neuronal death in SMA.

## MATERIALS AND METHODS

### Gene targeting, generation of loxP-flanked *SMN* exon 7 mice and mating

The targeting construct derived from 129Sv total genomic DNA was electroporated into embryonic stem (ES) cells, and of 406 G418-resistant ES cells two clones containing the specifically targeted allele (*SMN^F7^*) through homologous recombination were injected into blastocysts which were transferred into pseudopregnant foster mothers. One clone gave a high percentage of chimeras. Chimeras were bred to C57BL/6J females and mice harbouring the targeted allele were identified following genotype analysis of agouti offspring using two sets of primers: *PHR5-XG3* (5′-TTC TCT TGA TTC CCA CTT TGT GGT TC-3′; 5′-CTG GCC CAA ATC ACA ACA TAA-3′); or *ex7sou1-GS8* (5′-AGA AGG AAA GTG CTC ACA TAC AAA TT-3′; 5′-TGT CTA TAA TCC TCA TGC TAT GGA G-3′). Heterozygous *SMN^F7^* mice were intercrossed, and a strain homozygous for the *SMN^F7^* allele was established.

Mice heterozygous for the *SMN^F7^* allele were initially crossed with a strain carrying the *Cre* recombinase transgene driven by the CMV promoter (17). Offspring carrying both the *SMN^F7^* allele and *CMV-Cre* transgene were selected and crossed with C57BL/6J mice. A heterozygous deletion of the *SMN* exon 7 (*SMN^Δ7^*) was detected in offspring carrying both *CMV-Cre* and the mutated allele. Backcross of *CMV-Cre*, *SMN^Δ7/+^* with C57BL/6J mice allowed to select mice carrying a heterozygous deletion of *SMN* exon 7 in all cell types but lacking the *CMV-Cre* transgene (*SMN^Δ/+^*).

### Plasmid construction, generation of a Cre recombinase transgenic line and quantification of Cre-mediated deletion

A 2100 bp *Eco*RI–*Hin*dIII restriction fragment of the p*NSE-CAT* plasmid, containing the rat *NSE* gene promoter (18), was cloned into the pGS5 plasmid which contains the *Cre* recombinase gene separated from the promoter by the rabbit β-globin intron and followed by the *SV40* polyadenylation signal. Subsequently, the purified *Not*I fragment was microinjected into the pronuclei of fertilized eggs from (C57BL/6J × SJL) $F_1$ mice and implanted in pseudopregnant foster mothers. The parental transmission of the transgene was confirmed both by PCR amplification using primers *Cre1* (5′-CCG GTC GAT GCA ACG AGT GAT-3′) and *Cre2* (5′-ACC AGA GTC ATC CTT AGC GCC-3′) and Southern blotting. The PCR product (790 bp) was used as a probe for Southern blot analyses of DNA extracted from tail biopsy.

To test the efficiency of DNA excision by the Cre recombinase, transgenic mice were crossed with mice carrying the *SMN^F7^* allele and double transgenic mice were selected. Genomic DNA was extracted from a variety of adult tissues. The wild-type and *SMN^F7^* alleles were simultaneously amplified by PCR using one set of primers (*ex7sou1-GS8*). The efficiency of excision was estimated by comparing the intensity of the band amplified from the *SMN^F7^* allele with that of the band amplified from the wild-type allele which differs only in the absence of the loxP site. After 15 cycles, PCR products were separated by agarose gel electrophoresis, transferred to Nylon-$N^+$ membrane and hybridized using the

**Figure 5.** Skeletal muscle and spinal cord morphology of wild-type and *SMN^F7/Δ7^*, *Cre^+^* mice. (**A** and **B**) Haematoxylin and eosin staining of transverse sections of gastrocnemius muscle from 2-week-old mice. (**B** and **B′**) Groups of atrophic muscle fibers are evident in the mutant mouse compared with the diameter of muscle fibers of control muscle (A). (**B** and **B′**) In neighbouring areas, angular fibers (indicated by arrowhead) are intermixed with normal-appearing fibers. Neither necrosis, inflammatory cell infiltration nor fibrosis is observed. Scale bar, 20 μm. (**C** and **D**) Labeling of the acetylcholine receptors using rhodamine-conjugated α-bungarotoxin (AChR, 1:10000 dilution; Molecular Probes, Eugene, OR) on transverse sections of gastrocnemius muscle of 2-week-old wild-type and *SMN^F7/Δ7^*, *Cre^+^* mice. (**C**) In the control mouse, AChRs are concentrated at the neuromuscular junction with their characteristic α-bungarotoxin curved staining (arrow). (**D**) In *SMN^F7/Δ7^*, *Cre^+^* mice, a marked extrajunctional labeling of AChRs was observed in a pattern of expression characteristic for skeletal muscle denervation (29). Scale bar, 10 μm (C and D). (**E** and **I**) Toluidine blue staining of transverse semithin sections (1 μm) of spinal cord from 2-week-old mice. (**E** and **F**) In control mice, motor neurons are large cells of the anterior horns that contain abundant cytoplasm and a prominent nucleolus in a large rounded nucleus. (**G** and **I**) In *SMN^F7/Δ7^*, *Cre^+^* mice, note the abnormal morphology of the nuclei, which are characterized by the presence of indentations in the nuclear membrane of motor neurons. These indentations appear as intensely blue staining regions within the nuclei at the nuclear–cytoplasmic boundary (arrows). These abnormal nuclei are observed at different levels of the spinal cord including at the cervical, thoracic and lumbar levels. Note the granular aspect of motor neuron cytoplasm in (I). Scale bar, 4 μm.

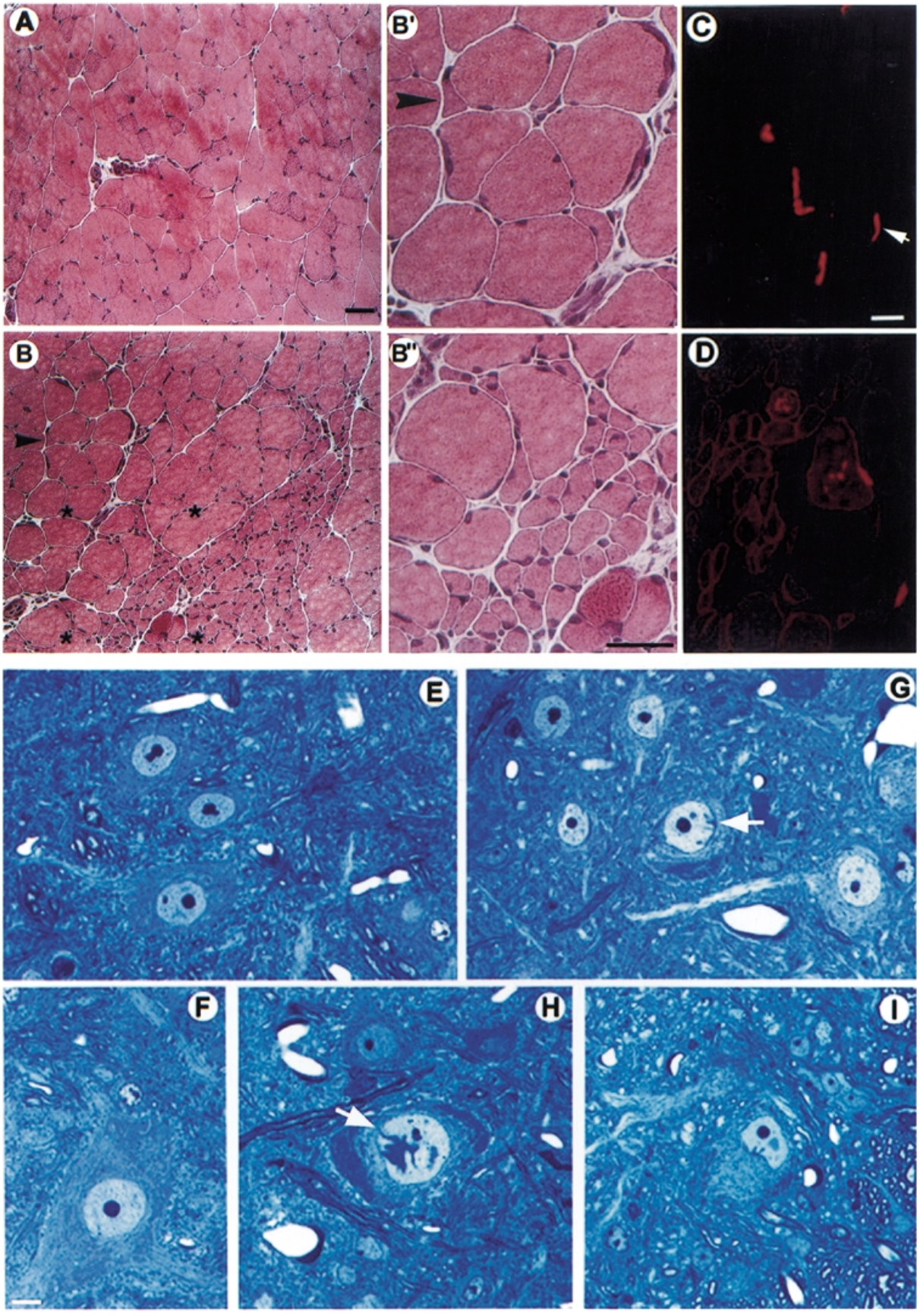
A
B'
C
B
B''
D
E
G
F
H
I

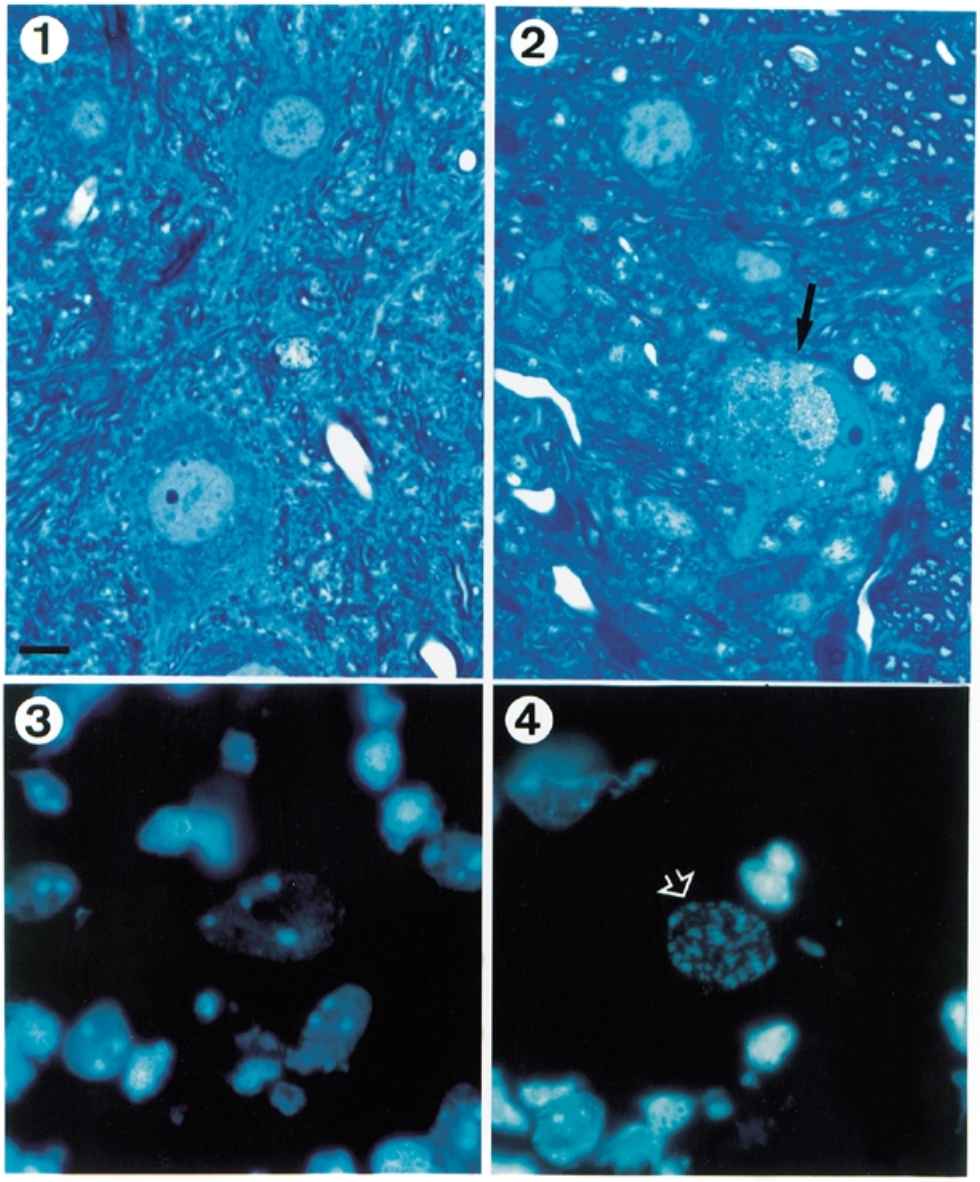


**Figure 6.** Spinal cord morphology of 4-week-old wild-type and $SMN^{F7/\Delta7}$, $Cre^{+}$ mice. Toluidine blue staining of transverse semithin sections (1 µm) of spinal cord of control (**1**) or mutant (**2**) mice. In addition to indentations of the nuclear membrane, the nucleus is markedly deformed in mutant mice (2). The motor neuron cytoplasm displays a granular aspect and is distended by accumulation of vacuoles (arrow). (**3** and **4**) DAPI staining of spinal cord section of control (3) or mutant mice (4) reveals fragmentation of the motor neuron nucleus in mutant mice. Scale bar, 4 µm.

wild-type PCR product as a probe. Intensity of bands was quantified using the Bio-Rad (Hercules, CA) GS700 densitometer and Molecular Analyst software.

For *in situ* hybridization experiments, a *Bam*HI–*Xho*I restriction fragment of the Cre recombinase gene derived from the pGS5 plasmid was subcloned into pBluescript plasmid KS(–). Sense and antisense RNA synthesis was performed using T3 or T7 RNA polymerase and labeled with [$\alpha$-$^{35}$S]CTP as previously described (28).

### Morphological and immunofluorescence analyses

For toluidine blue staining of the spinal cord, the mice were anaesthetized with nembutal and perfused with 0.9% NaCl and 2.5% glutaraldehyde, 0.5% paraformaldehyde in 0.1 M phosphate buffer (PB; pH 7.4). Tissue samples were dissected and immersed in the same fixative for 2 h, rinsed in PB and postfixed in 2% osmium tetroxide. After three washes with phosphate-buffered saline, each sample was dehydrated in a graded series of ethanol and embedded in Epon. Semithin transverse sections of spinal cord (1 µm) were stained with toluidine blue and examined under a Zeiss Axiophot microscope. Quantification of motor neuron number was performed at the lumbar level of the spinal cord using double labelling of nuclei and cytoplasm by DAPI and anti-choline acetyl transferase antibody (anti-ChAT, 1:800 dilution; Chemicon, Temecula, CA), respectively. Motor neurons were counted when large DAPI-stained nuclei-associated ChAT

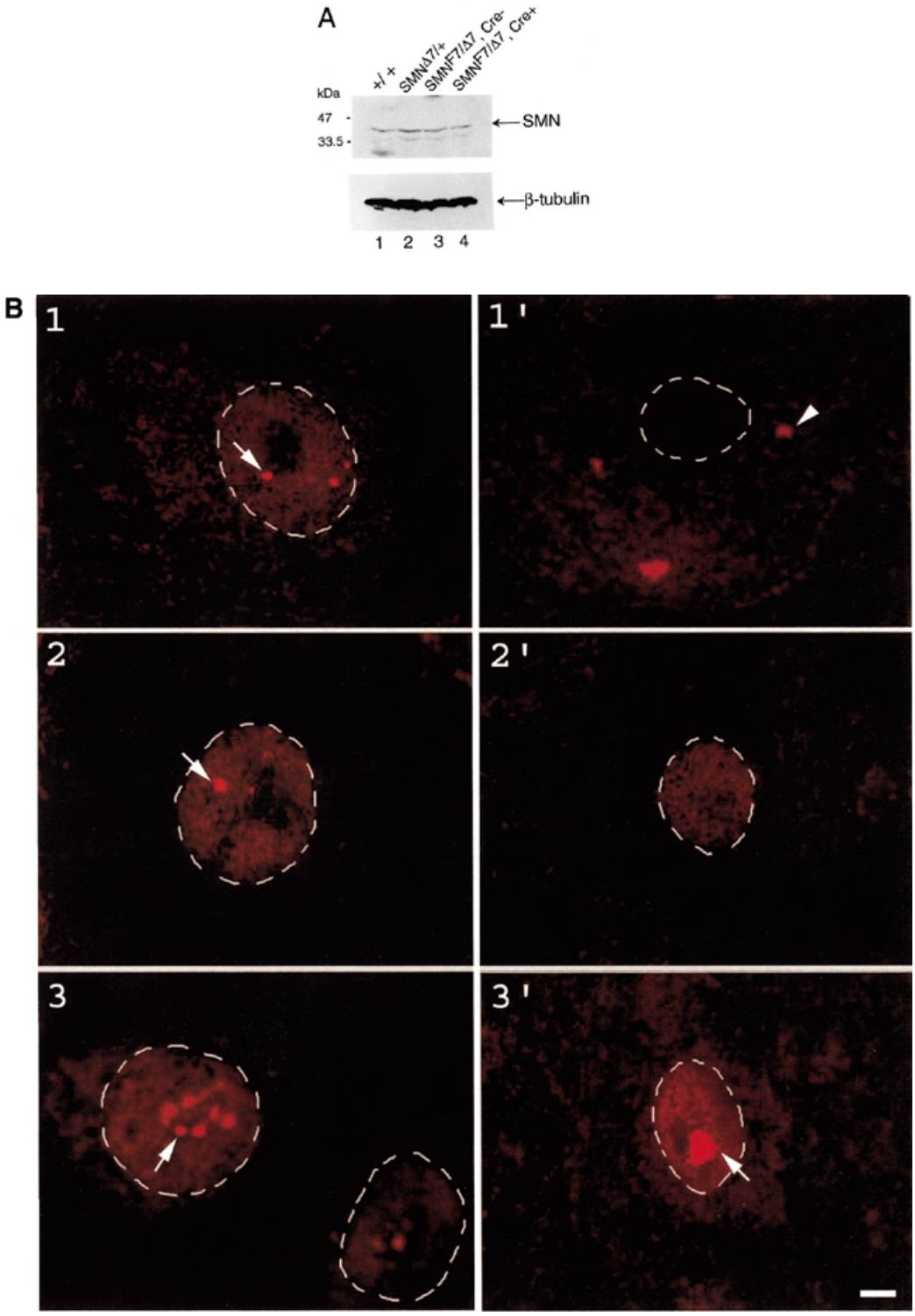


**Figure 7.** Immunostaining of SMN, SIP1 and coilin proteins. (**A**) Immunoblot analysis of total protein extracts from the spinal cord of wild-type and mutant mice was performed as previously described (25). The membranes were incubated with anti-SMN monoclonal antibody (1:2000 dilution) and anti-β-tubulin monoclonal antibody (1:5000 dilution; Amersham, Uppsala, Sweden) as an internal control. The membranes were washed and incubated with anti-mouse IgG conjugated to horseradish peroxidase and the immune complexes were revealed using chemiluminescent detection reagents (Pierce, Rockford, IL). (**B**) Confocal laser microscopy analysis of SMN (1 and 1′), SIP1 (2 and 2′), coilin (3 and 3′) on transverse spinal cord sections from wild-type (1, 2 and 3) and $SMN^{F7/\Delta7}$, $Cre^{+}$ mice (1′, 2′ and 3′). (1) In the control mouse, the 2B1 anti-SMN antibody stains both the cytoplasm and gems in the nuclei of motor neurons (arrow) whereas it fails to detect the nuclear staining of SMN-containing gems in $SMN^{F7/\Delta7}$, $Cre^{+}$ mice. Note the presence of aggregates in the cytoplasm (indicated by short arrow) (1′). (2) In the control, immunohistochemistry with the anti-SIP1 antibody (2E17) shows that SIP1 is concentrated in gems as previously described in HeLa cells (arrow). (2′) In $SMN^{F7/\Delta7}$, $Cre^{+}$ mice, note the absence of gems in motor neurons. (3) In the control, the anti-p80 coilin antibody (204,10) stains several coiled bodies in the nuclei of motor neurons (arrow), whereas it stains large nuclear aggregates in motor neurons of $SMN^{F7/\Delta7}$, $Cre^{+}$ (3′, arrow). Scale bars, 4 μm.

labelling of the cytoplasm were observed. Immunostaining of SMN, SIP1 and coilin was performed on tissues fixed with 4% paraformaldehyde and incubated with either monoclonal antibody anti-SMN (2B1, 1:500), anti-SIP1 (2E17, 1:100) or rabbit polyclonal anti-p80 coilin (204,10, 1:500) and revealed by Cy3-conjugated anti-mouse or rabbit IgG (Jackson Laboratories, West Grove, PA) then counterstained with DAPI. Confocal laser scanning microscopy analysis was performed using a Sarastro 2000 laser confocal system (Molecular Dynamics, Sunnyvale, CA) mounted on a Nikon Optiphot-2 upright microscope. Series of optical sections were taken at 0.2–0.3 μm steps.

## ACKNOWLEDGEMENTS

We are grateful to P. Kastner for providing the *PHR68* plasmid, D. Metzger for the *PGS5* plasmid and CMV-Cre transgenic strain, J. Sutcliffe for the *pNSE-CAT* plasmid, G. Dreyfuss for the anti-SMN and anti-SIP1 antibodies and J. Sleeman for the anti-p80 coilin antibody. We thank J.L. Mandel, A. Sobel and F. Rieger for invaluable help and Julia C. Young for useful comments. We thank the animal facility staff for animal care, the ES cell culture, microinjection and the sequencing facility services. We are grateful to J. Molgo and L. Faille for help in confocal laser microscopy analysis. All animal procedures were performed in accordance with institutional guidelines. This work was supported by the Institut National de la Santé et de la Recherche Médicale (INSERM), the Centre National de la Recherche Scientifique, the Hôpital Universitaire de Strasbourg, Rhône-Poulenc Rorer, the Association Française contre les Myopathies (AFM) and Families of SMA (USA). T.F., F.D.T., C.D. and P.M. are recipients of fellowships of Andrew's Buddies (USA), INSERM, GENOPOLE and Families of SMA (USA), respectively.

## REFERENCES

1. Pearn, J. (1973) The gene frequency of acute Werdnig–Hoffmann disease (SMA type I). A total population survey in North-East England. *J. Med. Genet.*, **10**, 260–265.
2. Pearn, J. (1978) Incidence, prevalence and gene frequency studies of chronic childhood spinal muscular atrophy. *J. Med. Genet.*, **15**, 409–413.
3. Melki, J., Lefebvre, S., Burglen, L., Burlet, P., Clermont, O., Millasseau, P., Reboullet, S., Zeviani, M., Le Paslier, D., Cohen, D. *et al.* (1994) *De novo* and inherited deletions in spinal muscular atrophies. *Science*, **264**, 1474–1477.
4. Lefebvre, S., Bürglen, L., Reboullet, S., Clermont, O., Burlet, P., Viollet, L., Benichou, B., Cruaud, C., Millasseau, P., Zeviani, M. *et al.* (1995) Identification and characterization of a spinal muscular atrophy-determining gene. *Cell*, **80**, 155–165.
5. Bürglen, L., Lefebvre, S., Clermont, O., Burlet, P., Viollet, L., Cruaud, C., Munnich, A. and Melki, J. (1996) Structure and organisation of the human survival motor neurone (*SMN*) gene. *Genomics*, **32**, 479–482.
6. Lorson, C.L., Hahnen, E., Androphy, E.J. and Wirth, B. (1999) A single nucleotide in the *SMN* gene regulates splicing and is responsible for spinal muscular atrophy. *Proc. Natl Acad. Sci. USA*, **96**, 6307–6311.
7. Lefebvre, S., Burglen, L., Frezal, J., Munnich, A. and Melki, J. (1998) The role of the SMN gene in proximal spinal muscular atrophy. *Hum. Mol. Genet.*, **7**, 1531–1536.
8. Liu, Q. and Dreyfuss, G. (1996). A novel nuclear structure containing the survival of motor neuron protein. *EMBO J.*, **15**, 3555–3565.
9. Fischer, U., Liu, Q. and Dreyfuss, G. (1997) The SMN–SIP1 complex has an essential role in spliceosomal snRNP biogenesis. *Cell*, **90**, 1023–1029.
10. Pellizzoni, L., Kataoka, N., Charroux, B. and Dreyfuss, G. (1998) A novel function for SMN, the spinal muscular atrophy disease gene product, in pre-mRNA splicing. *Cell*, **95**, 615–624.
11. Mattaj, I.W. (1998) Ribonucleoprotein assembly: clues from spinal muscular atrophy. *Curr. Biol.*, **8**, 93–95.
12. Viollet, L., Bertrandy, S., Bueno-Brunialti, A.L., Lefebvre, S., Burlet, P., Clermont, O., Cruaud, C., Guenet, J.L., Munnich, A. and Melki, J. (1997) cDNA isolation, expression, and chromosomal localization of the mouse survival motor neuron gene (*SMN*). *Genomics*, **40**, 185–188.
13. DiDonato, C.J., Chen, X.N., Noya, D., Korenberg, J.R., Nadeau, J.H. and Simard, L.R. (1997) Cloning, characterization, and copy number of the murine survival motor neuron gene: homolog of the spinal muscular atrophy-determining gene. *Genome Res.*, **7**, 339–352.
14. Schrank, B., Götz, R., Gunnersen, J.M., Ure, J.M., Toyka, K.V., Smith, A.G. and Sendtner, M. (1997) Inactivation of the survival motor neuron gene, a candidate gene for human spinal muscular atrophy, leads to massive cell death in early mouse embryos. *Proc. Natl Acad. Sci. USA*, **94**, 9920–9925.
15. Sternberg, N. and Hamilton, D. (1981) Bacteriophage P1 site-specific recombination. I. Recombination between loxP sites. *J. Mol. Biol.*, **150**, 467–486.
16. Sauer, B. and Henderson, N. (1988) Site-specific DNA recombination in mammalian cells by the Cre recombinase of bacteriophage P1. *Proc. Natl Acad. Sci. USA*, **85**, 5166–5170.
17. Dupe, V., Davenne, M., Brocard, J., Dolle, P., Mark, M., Dierich, A., Chambon, P. and Rijli, F.M. (1997) *In vivo* functional analysis of the Hoxa-1 3′ retinoic acid response element (3′RARE). *Development*, **124**, 399–410.
18. Forss-Petter, S., Danielson, P.E., Catsicas, S., Battenberg, E., Price J., Nerenberg, M. and Sutcliffe, J.G. (1990) Transgenic mice expressing β-galactosidase in mature neurons under neuron-specific enolase promoter control. *Neuron*, **5**, 187–197.
19. Andrade, L.E., Chan, E.K., Raska, I., Peebles, C.L., Roos, G. and Tan, E.M. (1991) Human autoantibody to a novel protein of the nuclear coiled body: immunological characterization and cDNA cloning of p80-coilin. *J. Exp. Med.*, **173**, 1407–1419.
20. Byers, R.K. and Banker, B.Q. (1961) Infantile spinal muscular atrophy. *Arch. Neurol.*, **5**, 140–164.
21. Davies, S.W., Turmaine, M., Cozens, B.A., DiFiglia, M., Sharp, A.H., Ross, C.A., Scherzinger, E., Wanker, E.E., Mangiarini, L. and Bates, G.P. (1997) Formation of neuronal intranuclear inclusions underlies the neurological dysfunction in mice transgenic for the HD mutation. *Cell*, **90**, 537–548.
22. Monani, U.R., Sendtner, M., Coovert, D.D., Parsons, D.W., Andreassi, C., Le, T.T., Jablonka, S., Schrank, B., Rossol, W., Prior, T.W. *et al.* (2000) The human centromeric survival motor neuron gene (*SMN2*) rescues embryonic lethality in *Smn*$^{-/-}$ mice and results in a mouse with spinal muscular atrophy. *Hum. Mol. Genet.*, **8**, 333–339.
23. Henderson, C.E., Hauser, S.L., Huchet, M., Dessi, F., Hentati, F., Taguchi, T., Changeux, J.P. and Fardeau, M. (1987) Extracts of muscle biopsies from patients with spinal muscular atrophies inhibit neurite outgrowth from spinal neurons. *Neurology*, **37**, 1361–1364.
24. Braun, S., Croizat, B., Lagrange, M.C., Warter, J.M. and Poindron, P. (1995) Constitutive muscular abnormalities in culture in spinal muscular atrophy. *Lancet*, **345**, 694–695.
25. Lefebvre, S., Burlet, P., Liu, Q., Bertrandy, S., Clermont, O., Munnich, A., Dreyfuss, G. and Melki, J. (1997) Correlation of severity with the SMN protein level in spinal muscular atrophy. *Nature Genet.*, **16**, 265–269.
26. Hsieh-Li, H.M., Chang, J.G., Jong, Y.J., Wu, M.H., Wang, N.M., Tsai, C.H. and Li, H. (2000) A mouse model for spinal muscular atrophy. *Nature Genet.*, **24**, 66–70.
27. Jablonka, S., Schrank, B., Kralewski, M., Rossoll, W. and Sendtner, M. (2000) Reduced survival motor neuron (*Smn*) gene dosage in mice leads to motor neuron degeneration: an animal model for spinal muscular atrophy type III. *Hum. Mol. Genet.*, **8**, 341–346.
28. Niederreither, K. and Dollé, P. (1998) *In situ* hybridization with $^{35}$S-labeled probes for retinoid receptors. *Methods Mol. Biol.*, **89**, 247–267.
29. Ko, P.K., Anderson, M.J. and Cohen, M.W. (1977) Denervated skeletal muscle fibers develop discrete patches of high acetylcholine receptor density. *Science*, **196**, 540–542.